Journal of Inorganic Biochemistry 147 (2015) 181–192

Contents lists available at ScienceDirect

Journal of Inorganic Biochemistry

journal homepage: www.elsevier.com/locate/jinorgbio

Mimicking peroxidase activity by a polymer-supported oxidovanadium(IV) Schiff base complex derived from salicylaldehyde and 1,3-diamino-2-hydroxypropane

Mannar R. Maurya [a,*], Nikita Chaudhary [a], Fernando Avecilla [b], Isabel Correia [c]

[a] Department of Chemistry, Indian Institute of Technology Roorkee, Roorkee 247667, India
[b] Departamento de Química Fundamental, Universidade da Coruña, Campus de A Zapateira, 15071 A Coruña, Spain
[c] Centro de Química Estrutural, Instituto Superior Técnico, Universidade de Lisboa, Av. Rovisco Pais 1 1049-001 Lisbon, Portugal

ARTICLE INFO

Available online 26 January 2015

Keywords:
Vanadium
Polymer-supported
Crystal structure
Peroxidase mimetic catalyst
Oxidation

ABSTRACT

The polymer-supported oxidovanadium(IV) complex PS-[$V^{IV}O$(sal-dahp)] (**2**) (PS = chloromethylated polystyrene crosslinked with 5% divinylbenzene, and H_3sal-dahp = dibasic pentadentate ligand derived from salicylaldehyde and 1,3-diamino-2-hydroxypropane) was prepared from the corresponding monomeric oxidovanadium(IV) complex [$V^{IV}O$(Hsal-dahp)(DMSO)] (**1**), characterized and successfully used as catalyst for the peroxidase-like oxidation of pyrogallol. The oxidation of pyrogallol to purpurogallin with PS-[$V^{IV}O$(sal-dahp)] (**2**) was achieved under mild conditions at pH 7 buffered solution. Plausible intermediate species formed during peroxidase mimicking experiments are proposed, by studying the model complex [$V^{IV}O$(Hsal-dahp)(DMSO)] (**1**) by UV–visible and ^{51}V NMR spectroscopies. The high peroxidase mimicking ability of polymer-supported complex **2**, its stability in a wide pH range, the easy separation from the reaction media, and the reusability without considerable decrease in activity, suggest that this heterogeneous catalyst has high potential for application in sustainable industrial catalysis.

1. Introduction

Peroxidase enzymes have important applications in many physiological reactions [1–7]. Peroxidase-like activity of haloperoxidases has also been reported towards classical peroxidase substrates using recombinant vanadium haloperoxidases [8]. However, the industrial application of natural or recombinant enzymes is not economically viable due to difficult bulk production, high costs, poor stability and very specific reaction conditions (such as pH and reaction medium). Applications of heterogeneous vanadium catalysts can potentially overcome these problems. The V_2O_5 nanowire [9] has been used as a heterogeneous catalyst mimicking peroxidase activity. However, to the best of our knowledge no examples of peroxidase like activity by polymer supported vanadium complexes have been reported so far.

The application of polymer supported vanadium complexes as catalysts has shown tremendous growth over the past few years [10,11]. Vanadium complexes in the presence of oxidants like H_2O_2 and *tert*-butylhydroperoxide (TBHP) are good oxidation catalysts as they easily form intermediate species containing an electron rich peroxido group, able to transfer oxygen to the organic substrate [12–14]. The polymer support mimics the protein mantle and prevents the decomposition of the complexes which in turn enhances the turn over numbers. These observations inspired us to design vanadium complexes covalently linked to Merrifield resin (chloromethylated polystyrene) to obtain biomimetic heterogeneous catalysts. Depending on the nature of ligands and metal complexes different strategies were implemented for the resin modification [10,11,15].

Smith et al. [16] prepared an oxidovanadium(IV) complex [$V^{IV}O$(Hsal-dahp)]$_n$ (H_3sal-dahp = dibasic pentadentate ligand derived from salicylaldehyde and 1,3-diamino-2-hydroxypropane) in which the ligand is similar to salen [17] but has an additional free hydroxyl group which can be used for immobilization on e.g. polystyrene. Despite showing good catalytic properties complex [$V^{IV}O$(Hsal-dahp)]$_n$ could not be immobilized on chloromethylated polystyrene due to its polymeric form, consisting of –(L)V═O–(L)V═O– chains. However, the complex can easily be converted into monomeric species using polar solvents like DMSO or DMF, which can then be immobilized on chloromethylated polystyrene.

In this contribution, we report the isolation of monomeric [$V^{IV}O$(Hsal-dahp)(DMSO)] complex, its immobilization on chloromethylated polystyrene and its characterization. The polymer supported complex (abbreviated as PS-[$V^{IV}O$(sal-dahp)]) shows good peroxidase-like activity in aqueous medium. The analogous complex [$V^{V}O$(hap-dahp)] (derived

* Corresponding author. Tel.: +91 1332 285327; fax: +91 1332 273560.
E-mail address: rkmanfcy@iitr.ac.in (M.R. Maurya).

http://dx.doi.org/10.1016/j.jinorgbio.2015.01.012
0162-0134/

from *o*-hydroxyacetophenone and 1,3-diaminohydroxypropane) has been encapsulated in the nanopores of zeolite-Y and applied as catalyst for oxidation reactions [18].

2. Experimental section

2.1. Materials and methods

V_2O_5, (Loba Chemie, India), 1,3-diamino-2-hydroxypropane (Aldrich, U.S.A.), salicylaldehyde (Sisco Research, India) and 30% aqueous H_2O_2 (Qualigens, India) were used as obtained. A gift sample of chloromethylated polystyrene [18.9% Cl (5.35 mmol Cl per gram of resin)] cross-linked with 5% divinylbenzene (PS-Cl) was obtained from Thermax Limited, Pune, India. All other chemicals and solvents used were of AR grade.

Vanadium content in PS-[$V^{IV}O$(sal-dahp)] (**2**) was determined by inductively coupled plasma–mass spectrometry (ICP–MS). The sample was prepared by taking 0.020 g of **2** and treating it with 6 mL of nitric acid–hydrochloric acid (1:1) mixture on a hot plate. After complete leaching the residue was dissolved in deionized-distilled water, filtered and diluted to 50 mL. Elemental analyses (C, H, N and S) of the complexes were obtained in an Elementar model Vario-EL-III. Thermal stability of neat, as well as, polymer-supported complexes was studied using a Perkin-Elmer (Pyris Diamond) thermogravimetric analyzer under oxygen atmosphere (flow rate: 200 mL/min, heating rate: 10 °C/min and temperature range: 35–1000 °C) using alumina powder as reference. IR spectra with 2 cm^{-1} resolution were recorded as KBr pellets on a Nicolet 1100 FT-IR spectrometer. Electronic absorption spectra of ligand and neat complex were recorded in methanol using a Shimadzu 1601 UV–visible (UV–vis) spectrophotometer. The spectrum of polymer-supported complex was recorded in Nujol by layering the sample mull inside a cuvette and keeping the reference cuvette layered with Nujol. EPR spectra were recorded with a Bruker ESP 300E X-band spectrometer coupled to a Bruker ER041 X-band frequency meter (9.45 GHz) and the spin Hamiltonian parameters were obtained by simulation of the spectra with the computer program of Rockenbauer and Korecz [19]. Complex **1** was dissolved in DMF (p.a. grade) (3 mM), previously degassed by passing N_2 for 10 min, and the solution was immediately frozen in liquid nitrogen. The EPR spectrum was measured at 77 K. The EPR spectrum of solid polymer-supported complex **2** was measured at room temperature in quartz tubes. ^{51}V NMR spectra of ca. 3 mM solutions of complex **1** in DMF (p.a. grade) (5% D_2O added) were recorded on a Bruker Avance III 400 MHz instrument. ^{51}V chemical shifts were referenced relative to neat $V^{V}OCl_3$ as external standard.

Atomic force microscopy (AFM) imaging was performed on a scanning probe microscope from NTEGRA (NT–MDT) in a semi-contact mode. The morphology and elemental analysis of both the cholоromethylated polystyrene and polymer supported complex were obtained by a FEI-Quanta 200 FEG field emission scanning electron microscope (FE-SEM) coupled with an energy dispersive X-ray analyses (EDAX) accessory. The sample was coated with a thin film of gold to prevent surface charging and to protect the surface material from thermal damage by electron beam. A uniform thickness of about 0.1 mm was maintained. A constant voltage of 20 kV was applied so that only the outer surface was accessible.

2.2. Synthesis

[$V^{IV}O(acac)_2$] [20] and H_3sal-dahp (**I**) [16] were prepared according to methods reported in the literature.

2.2.1. [$V^{IV}O$(Hsal-dahp)(DMSO)] (**1**)

The polymeric complex [$V^{IV}O$(Hsal-dahp)]$_n$ was prepared by reaction of $VOSO_4 \cdot 5H_2O$ (0.506 g, 2.00 mmol) and H_3sal-dahp (0.596 g, 2.00 mmol) in methanol as reported in the literature [16]. An alternative method was also used and is given here. To a stirred solution of H_3sal-dahp (0.596 g, 2.00 mmol) in methanol (10 mL) was added a solution of [$V^{IV}O(acac)_2$] (0.530 g, 2.00 mmol) in methanol (10 mL) and the reaction mixture was refluxed for 1 h, after which a light orange solid was formed. The solid was filtered, washed with methanol and dried in vacuum over silica gel. Yield: 0.580 g (80%).

Complex [$V^{IV}O$(Hsal-dahp)]$_n$ was dissolved in a minimum amount of hot DMSO, filtered and left for slow evaporation at room temperature. An orange solid slowly precipitated which was filtered and dried in a vacuum desiccator over silica gel. Anal. Calc. for $C_{19}H_{22}N_2O_5SV$ ([$V^{IV}O$(Hsal-dahp)(DMSO)]) (441.39): C, 51.70; H, 5.02; N, 6.34; S, 7.26%. Found: C, 52.13; H, 4.92; N, 6.50; S, 6.94%.

Light orange crystals of [$V^{IV}O$(Hsal-dahp)(DMSO)]$\cdot H_2O$ (**1**$\cdot H_2O$) suitable for X-ray diffraction study were grown from DMSO, which were filtered and dried at room temperature.

2.2.2. PS-[$V^{IV}O$(sal-dahp)] (**2**)

Cholоromethylated polystyrene beads (1.0 g) were suspended in DMF (20 mL) and left for 2 h. A solution of [$V^{IV}O$(Hsal-dahp)(DMSO)] (1.0 g, 2.3 mmol) in DMF (30 mL) was added to the above suspension of beads. After adding triethylamine (3 mL) and K_2CO_3 (0.069 g, 0.50 mmol) the resulting mixture was heated at 90 °C for 2 days with slow mechanical stirring. Finally, the beads were filtered off, washed with DMF, followed by hot methanol and dried at 80 °C. Recovery yield: 94%. Vanadium content found by ICP–MS: 0.145 mmol g^{-1} of resin.

2.3. Peroxidase mimetic activity: catalytic oxidation of pyrogallol

Catalyst PS-[$V^{IV}O$(sal-dahp)] was suspended in acetonitrile for 2 h before starting the reaction. The peroxidase mimetic activity was determined using UV–vis spectrophotometry by monitoring the absorbance increase at 420 nm (due to the formation of purpurogallin, $\varepsilon = 2640\ M^{-1}\ cm^{-1}$) for up to 2 h [9,28]. The reaction was carried out in 3 mL of phosphate buffer (1 M, pH 7). The reaction was started with the addition of 1 mL of 0.25×10^{-1} M solution of 30% H_2O_2 to 1 mL of 0.25×10^{-1} M pyrogallol solution and catalyst PS-[$V^{IV}O$(sal-dahp)] (0.007 g). The steady state kinetics were done by varying the concentration of pyrogallol (0.2–1.4 mM) while keeping a fixed concentration of H_2O_2 (0.25×10^{-6} M) and catalyst PS-[$V^{IV}O$(sal-dahp)] (0.007 g). The reaction was carried out in 2 mL phosphate buffer (1 M, pH 7) and monitored spectrophotometrically by measuring the formation of purpurogallin at 420 nm ($\varepsilon = 2640\ M^{-1}\ cm^{-1}$) in time scan

Table 1
Crystal data and structure refinement for [$V^{IV}O$(sal-dahp)(DMSO)]$\cdot H_2O$ (**1**$\cdot H_2O$).

	1$\cdot H_2O$
Formula	$C_{19}H_{24}N_2O_6SV$
Formula weight	459.40
T, *K*	100(2)
Wavelength, Å	0.71073
Crystal system	Orthorhombic
Space group	Pnma
a/Å	16.9139(5)
b/Å	15.8319(4)
c/Å	7.3289(2)
V/Å^3	1962.53(9)
Z	4
F_{000}	956
D_{calc}/g cm^{-3}	1.555
μ/mm^{-1}	0.652
θ/(°)	2.73 to 28.32
R_{int}	0.0376
Crystal size/mm^3	0.22 × 0.19 × 0.15
Goodness-of-fit on F^2	1.063
$R_1[I > 2\sigma(I)]$[a]	0.0284
R_w (all data)[b]	0.0780
Largest differences peak and hole (eÅ^{-3})	0.412 and −0.368

[a] $R_1 = \Sigma||F_o| - |F_c||/\Sigma|F_o|$.
[b] $R_w(F^2) = \{\Sigma[w(F_o^2 - F_c^2)^2]/\Sigma[w(F_o^2)^2]\}^{1/2}$.

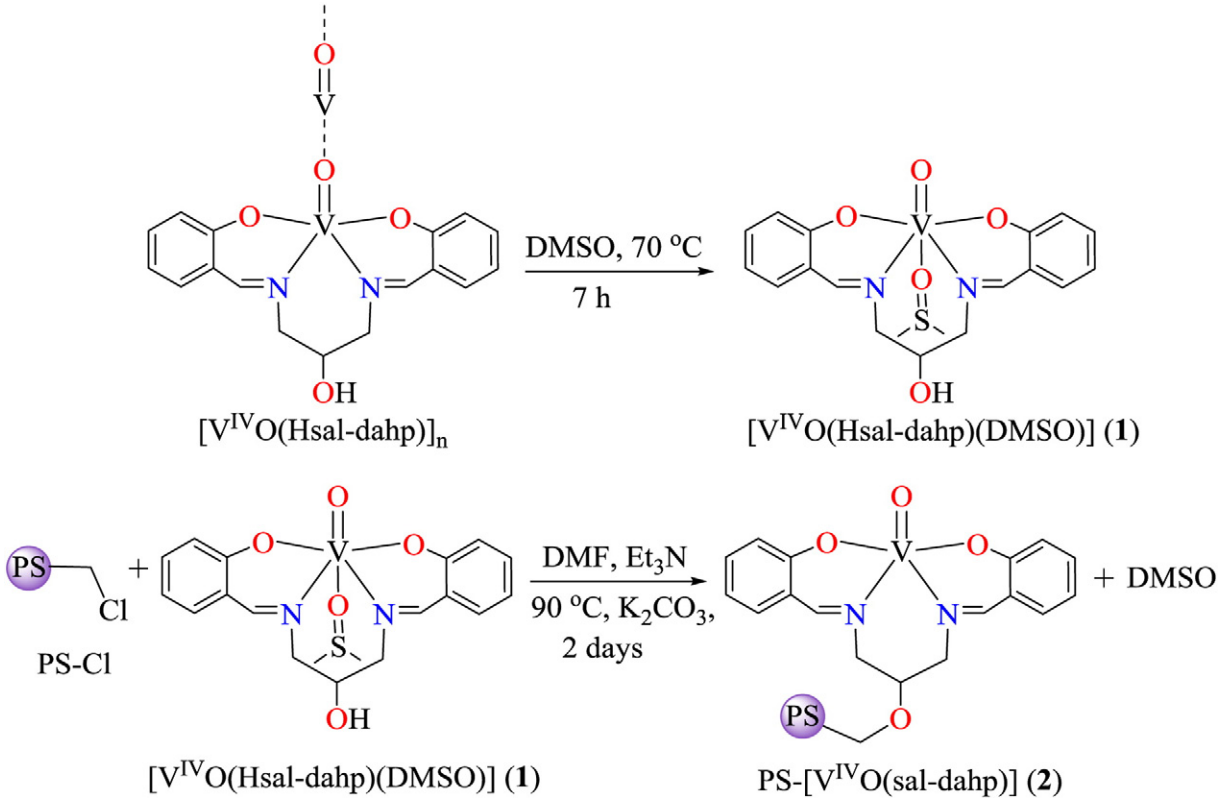

Scheme 1. General synthetic route for the preparation of monomeric vanadium complex [V^{IV}O(Hsal-dahp)(DMSO)] (**1**) and its polymer-supported complex PS-[V^{IV}O(sal-dahp)] (**2**). PS represents the backbone of the chloromethylated polystyrene.

mode. The initial reaction rates were fitted to Michaelis–Menten equation and calculated. Lineweaver–Burk linearizations were performed using Sigma-Plot software (Systat Software Inc.) with enzyme kinetics module to determine kinetic parameters.

2.4. X-ray crystal structure determination

Three-dimensional X-ray data were collected on a Bruker Kappa Apex CCD diffractometer at low temperature for **1**·H_2O by the ϕ–ω scan method. Reflections were measured from a hemisphere of data collected from frames each of them covering 0.3° in ω. Of the 18,878 reflections measured, all were corrected for Lorentz and polarization effects and for absorption by multi-scan methods based on symmetry-equivalent and repeated reflections. A total of 2200 independent reflections exceeded the significance level ($|F|/\sigma|F| > 4.0$. Complex scattering factors were taken from the program package SHELXTL [21]. The structure was solved by direct method and refined by full matrix least-squares on F^2. Hydrogen atoms were left to refine freely.

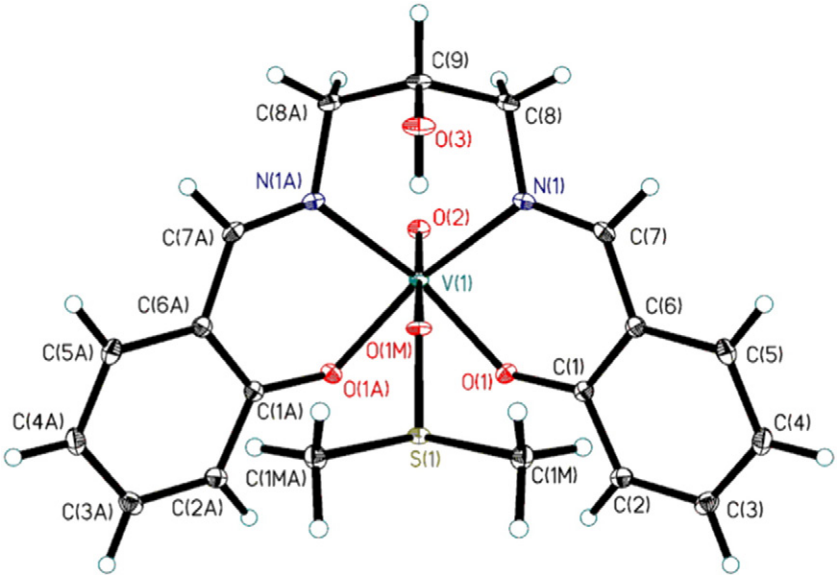

Fig. 1. ORTEP representation of [V^{IV}O(Hsal-dahp)(DMSO)]· H_2O (**1** · H_2O) showing the atom labeling scheme. The ligand coordinates through the two imine-N and two phenolate-O atoms, with the hydroxyl-O atom protonated and not taking part in coordination. The thermal ellipsoids are drawn at 30% probability level.

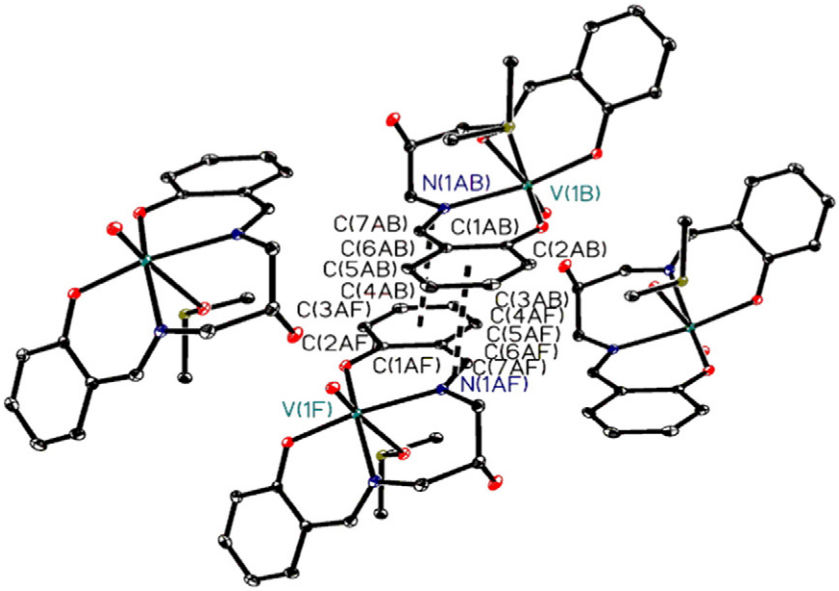

Fig. 2. ORTEP representation of the crystal packing in $[V^{IV}O(Hsal\text{-}dahp)(DMSO)]\ H_2O$ (**1** H_2O) evidencing the π–π interactions between phenol rings and C═N bonds of neighbor molecules.

Refinements were done with allowance for thermal anisotropy of all non-hydrogen atoms. Further details of the crystal structure determination are given in Table 1. A final difference Fourier map showed no residual density outside: 0.412 and −0.368 e.Å^{-3}. A weighting schemew = 1 / $[\sigma^2(F_o^2) + (0.038600\ P)^2 + 1.162400\ P]$, where P = $(|F_o|^2 + 2|F_c|^2) / 3$, was used in the latter stages of refinement.

3. Results and discussion

Reaction between $[V^{IV}O(acac)_2]$ (Hacac = acetylacetone) and tribasic pentadentate Schiff base H_3sal-dahp (**I**) in methanol leads to the formation of an oxidovanadium(IV) complex where the ligand acts as dibasic tetradentate and coordinates through the phenolic oxygen atoms and the azomethine nitrogen atoms. The hydroxyl oxygen of the ligand is not involved in the metal coordination. The complex is polymeric in nature, having the formula $[V^{IV}O(Hsal\text{-}dahp)]_n$ in the solid state, with polymeric chains of V═O–V═O [16]. Dissolving $[V^{IV}O(Hsal\text{-}dahp)]_n$ in hot (80 °C) DMSO and leaving it for crystallization at room temperature results in breaking of the V═O–V═O chains, yielding the monomeric species $[V^{IV}O(Hsal\text{-}dahp)(DMSO)]$ (**1**); Scheme 1.

Reaction of chloromethylpolystyrene cross-linked with 5% divinylbenzene (PS-Cl) with complex **1** in DMF, in the presence of triethylamine, resulted in the formation of the corresponding polymer-grafted oxidovanadium(IV) complex, PS-$[V^{IV}O(sal\text{-}hdap)]$ (**2**); Scheme 1. Complexes were characterized by spectroscopic techniques (IR, UV–vis and EPR), thermogravimetry, AFM and FE-SEM as well as EDAX studies.

Table 2
Selected bond lengths [Å] and angles [°] for $[V^{IV}O(Hsal\text{-}dahp)(DMSO)]\cdot H_2O$ (**1**·H_2O).

Bond lengths	**1**·H_2O
V(1)–O(1)	1.9571(10)
V(1)–O(2)	1.6025(15)
V(1)–N(1)	2.1064(12)
V(1)–O(1 M)	2.3177(14)
N(1)–C(7)	1.280(2)
N(1)–C(8)	1.4647(18)
Bond angles	**1**·H_2O
O(2)–V(1)–O(1)	104.55(5)
O(2)–V(1)–N(1)	95.31(5)
O(1)–V(1)–N(1)	87.89(4)
O(2)–V(1)–O(1 M)	167.21(6)
O(1)–V(1)–O(1 M)	84.78(4)
N(1)–V(1)–O(1 M)	76.03(4)

3.1. TGA studies

The thermal stability of neat (**1**) and polymer-supported (**2**) complexes was studied by thermogravimetric analysis. The neat complex $[V^{IV}O(Hsal\text{-}dahp)(DMSO)]$ (**1**) is stable up to ca. 160 °C. Thereafter, the decomposition of the organic part occurs in three consecutive exothermic steps and the final residue (21.0% at ca. 500 °C) corresponds to V_2O_5. The theoretical value (20.5%) is close to the experimentally obtained one. The thermal decomposition of PS-$[V^{IV}O(sal\text{-}dahp)]$ (**2**) occurs in three steps. The weight loss of 4.8%, observed in the 100–200 °C temperature range, may be due to loss of trapped solvent and water molecules. The weight loss in the 200–400 °C temperature range is possibly due to partial collapse of the complex moiety. Major decomposition occurs between 400 and 500 °C, which is tentatively attributed to decomposition of the major part of the polymer residue along with decomposition of the remaining part of the organic ligand. Further weight loss of 1.8% was observed between 500 and 900 °C. The final residue of 0.9% is due to V_2O_5 and the vanadium content calculated from this value is 0.17 mmol g^{-1} of resin, which is roughly in agreement with the vanadium content obtained from ICP–MS (0.145 mmol g^{-1} of resin) and EDAX (0.127 mmol g^{-1} of resin).

Table 3
Hydrogen bonds parameters for $[V^{IV}O(Hsal\text{-}dahp)(DMSO)]\cdot H_2O$ (**1**·H_2O).

D–H…A	d(D–H)	d(H…A)	d(D…A)	<(DHA)
O(1 W)–H(2WA)…O(3)#2	0.88(4)	1.91(4)	2.793(2)	175(3)
O(1 W)–H(1WA)…O(1)#3	0.81(5)	2.51(4)	3.195(2)	143(2)
O(1 W)–H(1WA)…O(1)#4	0.81(5)	2.51(4)	3.195(2)	143(2)
O(3)–H(3O)…O(1 M)	0.80(3)	2.11(3)	2.902(2)	172(3)

Symmetry transformations used to generate equivalent atoms:
#1 x,−y + 1/2,z #2 x + 1/2,y,−z + 5/2 #3 x,−y + 1/2,z + 1 #4 x,y,z + 1.

Table 4
Selected IR (cm^{-1}) and electronic absorption spectral data (nm) of ligand and complexes.

Compounds	ν(OH)	ν(C═N)	ν(V═O)	λ_{max}/nm (ε/M^{-1} cm^{-1})
H_3sal-dahp (**I**)	3390 (br)[a]	1607	–	215 (4.4×10^4), 256 (2.3×10^4), 282 (0.6×10^4), 316 (0.8×10^4), 402 (2.2×10^3)[b]
[V^{IV}O(Hsal-dahp)(DMSO)] (**1**)	3386	1597	950	232 (4.4×10^4), 270 (2.2×10^4), 361 (8.2×10^3)[b] 488 (98), 748 (7)[c]
PS-[V^{IV}O(sal-dahp)] (**2**)	3400 (br)[a]	1604	965	280, 386, 515[d]

[a] br = broad.
[b] In MeOH.
[c] In DMF.
[d] In Nujol.

3.2. Structure description of [V^{IV}O(Hsal-dahp)(DMSO)]·H_2O (**1**·H_2O)

An orange prism of [V^{IV}O(Hsal-dahp)(DMSO)]·H_2O (**1**·H_2O) crystallizes in a centrosymmetric orthorhombic space group, Pnma. One half water molecule and one half [V^{IV}O(Hsal-dahp)(DMSO)] complex are present in the asymmetric unit and grow through x, −y + 1/2, z (#1) symmetry transformation for the generation of equivalent atoms. The complex adopts a six-coordinated structure with distorted octahedral geometry. The phenolic oxygen and the imine nitrogen atoms of the ligand coordinate the vanadium center while the hydroxyl group does not participate in the coordination. One DMSO molecule and one oxido group complete the coordination sphere. The equatorial plane therefore comprises the [N(1), O(1), N(1A), O(1A)] donor atom set, and the $V^{V}O$ center stands above this plane by 0.3455(12) Å.

Fig. 1 shows an ORTEP representation of **1**·H_2O and Fig. 2 shows the crystal packing in which the complex forms an antiparallel dimer through π–π interactions between phenol rings and C═N bonds of neighboring molecules. Table 2 presents selected bond lengths and angles. The distances between centroids are: d_{c1-c2} = 3.457 Å [c1 (C7AB–N1AB), c2 (C1AF–C2AF–C3AF–C4AF–C5AF–C6AF)], d_{c3-c4} = 3.457 Å [c3 (C7AF–N1AF), c4 (C1AB–C2AB–C3AB–C4AB–C5AB–C6AB)]. Intermolecular hydrogen bonds between water molecules and complexes are present in the crystal packing (see Table 3). An intramolecular hydrogen bond is present between the hydroxyl group and the coordinated DMSO molecule.

3.3. IR spectral studies

IR spectra of the ligand (H_3sal-dahp), [V^{IV}O(Hsal-dahp)(DMSO)], PS-Cl and PS-[V^{IV}O(sal-dahp)] are shown in supporting information (SI, Fig. SI–1A and 1B) and selected bands and its tentative assignment are presented in Table 4. The ligand spectrum displays a broad band at 3390 cm^{-1} due to free —OH groups. The bonding of hydroxyl oxygen to PS-Cl could not be ascertained by IR spectroscopy as PS-[V^{IV}O(sal-dahp)] (**2**) also exhibits a weak broad band at 3400 cm^{-1} due to trapped residual water in the polymer matrix. The band at 1607 cm^{-1}, due to the azomethine group, shifts to lower wavenumbers in both complexes, corroborating the coordination of the nitrogen to the vanadium center. Neat complex **1** exhibits a sharp band at ca. 950 cm^{-1} due to monomeric ν(V═O) stretching mode, while the supported complex presents this band at 965 cm^{-1}. Other characteristic bands due to polystyrene are also present in the spectrum of the supported complex (see SI).

3.4. Electronic spectral studies

Electronic absorption spectra of a similar ligand (H_3hap-dahp), its vanadium complex and zeolite-Y encapsulated complex have been described in the literature [18]. The spectral data for the ligand H_3sal-dahp (**I**) and its neat as well as polymer-grafted vanadium complex are presented in Table 4; Fig. 3 (a and b) presents the electronic absorption spectra. All ligand bands appear in the spectra of the complexes with shifts in their positions. Bands due to d–d transitions for [V^{IV}O(Hsal-dahp)(DMSO)] (**1**) become clearer in DMF and have λ_{max} at 488 (ε/M^{-1} cm^{-1} = 98) and 748 nm (ε/M^{-1} cm^{-1} = 7). The

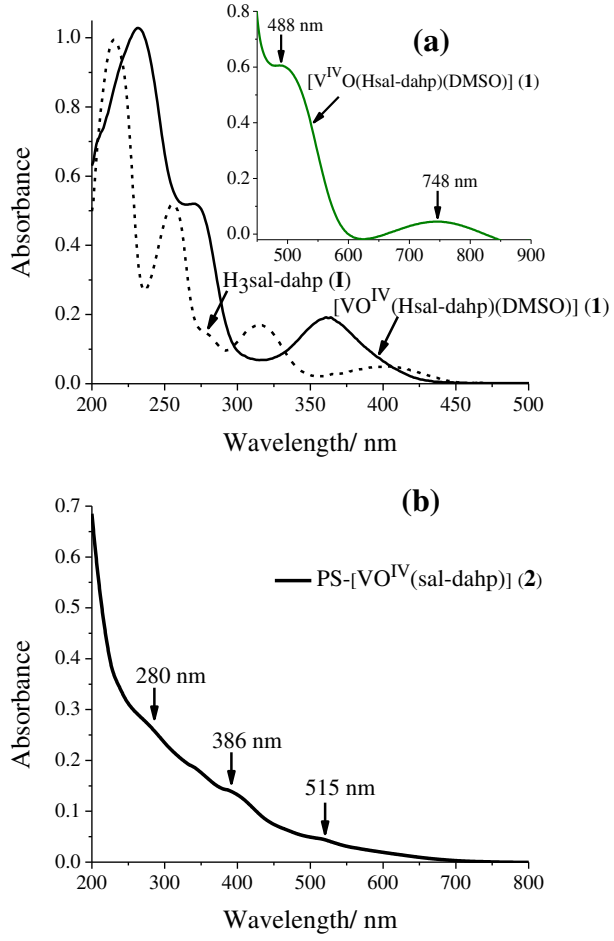

Fig. 3. Electronic absorption spectra of (a): H_3sal-dahp (**I**) and [V^{IV}O(Hsal-dahp)(DMSO)] (**1**) recorded in methanol. Inset shows spectrum of **1** in DMF in the visible region; (b): PS-[VO^{IV}(sal-dahp)] (**2**) recorded in Nujol®.

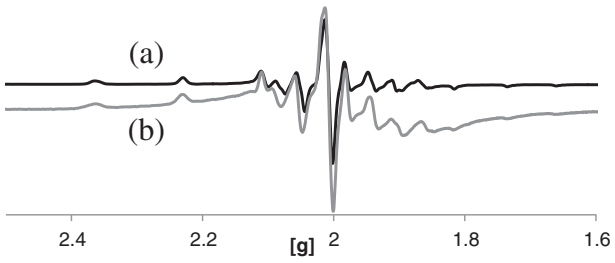

Fig. 4. 1st derivative X-band EPR spectra of [VO^{IV}(Hsal-dahp)(DMSO)] (**1**) (a) recorded from DMF solution at 77 K, and of PS-[VO^{IV}(sal-dahp)] (**2**) (b) recorded from neat solid at room temperature.

Table 5
Spin Hamiltonian parameters obtained from simulation of the EPR spectra of complexes **1** and **2**.

Complex	g	$A \times 10^4$ cm^{-1}	$g_{//}$	$A_{//} \times 10^4$ cm^{-1}
[V^{IV}O(Hsal-dahp)(DMSO)] (**1**)	1.983	53.9	1.956	158.9
PS-[V^{IV}O(sal-dahp)] (**2**)	1.981	57.3	1.951	160.9

polymer-supported complex PS-[V^{IV}O(sal-dahp)] (**2**) exhibits a ligand to metal charge transfer (LMCT) band at 386 nm (Fig. 3b). In addition, one d–d band at 515 nm could also be identified.

3.5. EPR spectral study

The 1st derivative EPR spectra of a "frozen" (77 K) solution of [V^{IV}O(Hsal-dahp)(DMSO)] (**1**) in DMF (4.7×10^{-3} M) and of solid PS-[V^{IV}O(sal-dahp)] (**2**) at room temperature are compared and presented in Fig. 4. The spectra of both complexes are well resolved. The spectrum of **2** is characteristic of magnetically diluted V^{IV}O-complexes and the well-resolved EPR hyperfine features indicate that the vanadium(IV) centers are well dispersed in the polymer matrix. Both spectra were simulated and the obtained spin Hamiltonian parameters $g_{//}$ and $A_{//}$ (Table 5) are similar for both compounds confirming a similar donor set for the neat and the PS-complex. The $A_{//}$ parameters are also in agreement with the value estimated using the additivity relationship proposed by Wüthrich [22] and Chasteen [23] (with estimated accuracy of $\pm 3 \times 10^{-4}$ cm^{-1}), which is 161×10^{-4} cm^{-1}, considering the equatorial donor set {$2 \times N_{imine}$, $2 \times O_{phenolate}$} [17,22,23]. The predicted contributions to the parallel hyperfine coupling constant for the donor groups under consideration are the same. EPR does not help in the assignment of the apical donor, since the unpaired electron probably occupies a d_{xy} orbital, which has its lobes in the equatorial plane. Therefore, a molecule of DMSO might be present in the apical position of the PS-complex, as it is in the neat complex.

3.6. Field emission-scanning electron microscope (FE-SEM) and energy dispersive X-ray analysis (EDAX) studies

Micrographs of chloromethylated polystyrene (PS-Cl) beads and PS-[V^{IV}O(sal-dahp)] beads (**2**) were recorded and their images are shown in Fig. 5 (a and b). Only small morphological changes were observed among plain polymer beads (PS-Cl) and polymer-anchored complex. However, a considerable increase in the diameter of beads was noticed. After complex anchoring EDAX (Fig. 5 (a′ and b′)) analysis shows 0.13 ± 0.03 mmol g^{-1} of resin of average vanadium content on the surface, which is in agreement with the value obtained with ICP–MS (0.145 mmol g^{-1}).

3.7. Atomic force microscopic (AFM) study

The morphological changes of PS-Cl (Fig. 6) after anchoring of complex were also studied by measuring the surface roughness using AFM. The surface roughness and mean height for PS-Cl were 7.28 nm and 72.8 nm, respectively. Upon reaction of PS-Cl with [V^{IV}O(Hsal-dahp)(DMSO)], the surface roughness and mean height decreased to 1.92 nm and 13.8 nm, respectively. This shows that the complex was anchored in the bead's pores, thereby reducing its porosity [24–26].

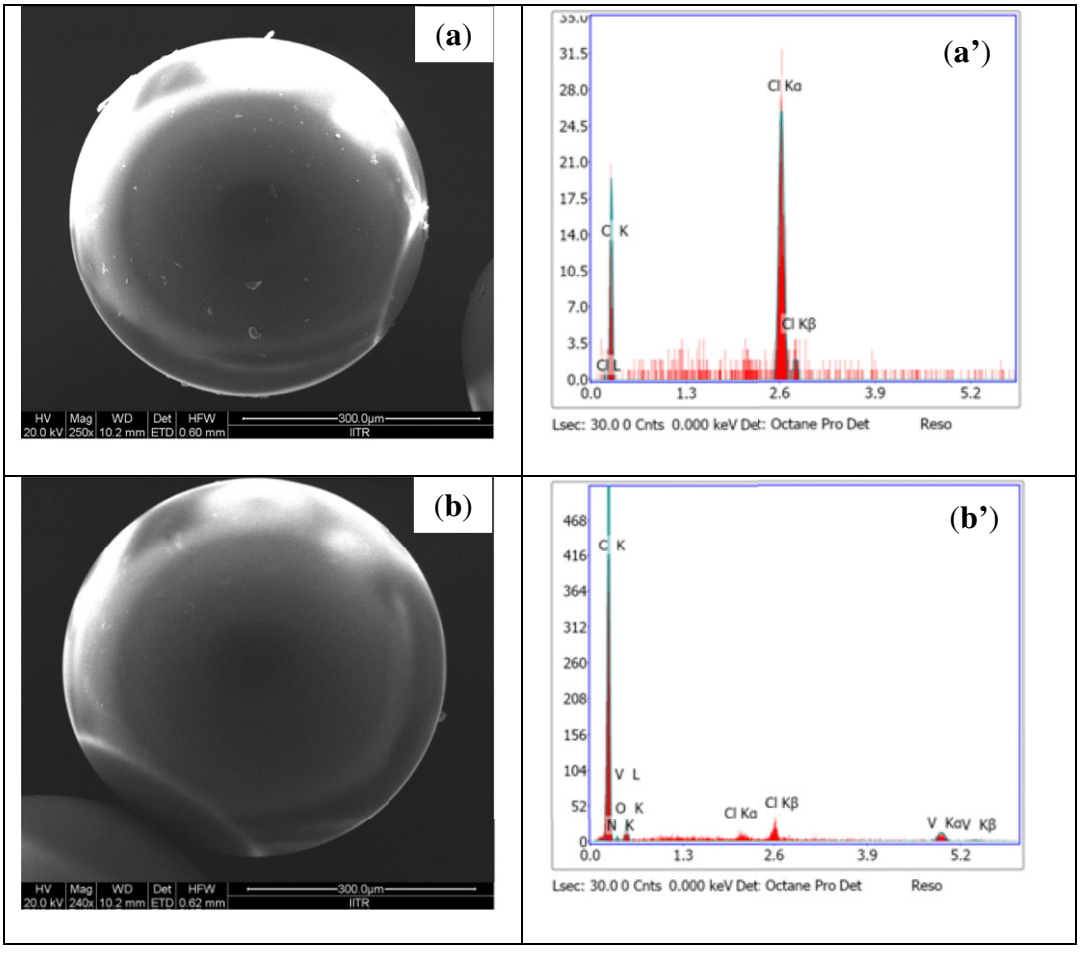

Fig. 5. Field emission scanning electron micrographs of PS-Cl (a) and PS-[V^{IV}O(sal-dahp)] (b) and the energy dispersive X-ray analysis graphs of PS-Cl (a′) and PS-[V^{IV}O(sal-dahp)] (b′).

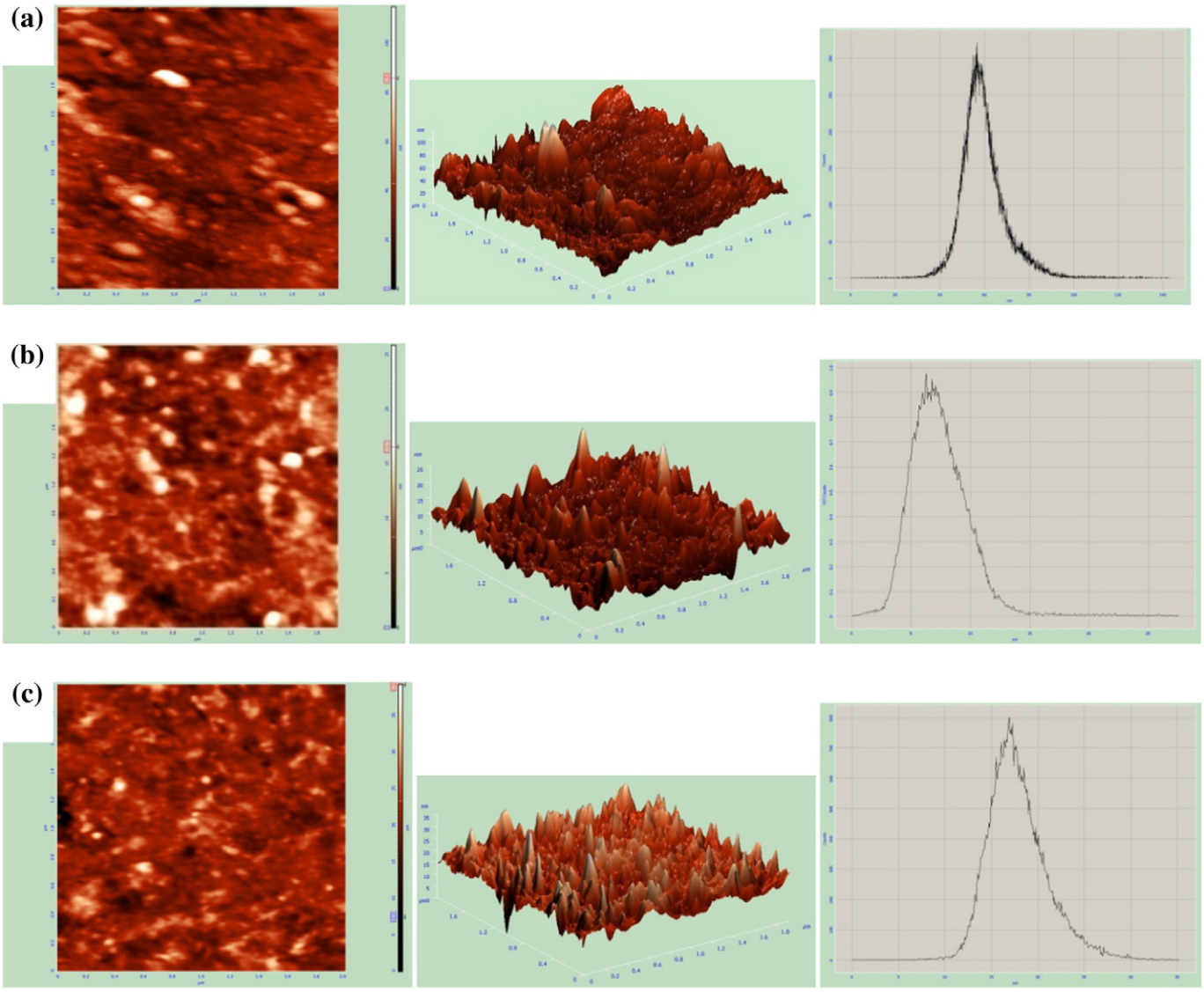

Fig. 6. AFM images (left), 3d-views (middle) and respective histograms (right) of (a): PS-Cl, (b): PS-[$V^{IV}O$(sal-dahp)] and (c) PS-[$V^{IV}O$(sal-dahp)] after 4 oxidation cycles. Scanning area 2×2 μM.

The morphology of the PS-complex **2** was also evaluated after 4 catalytic cycles, showing small increase in the surface roughness and mean height (2.45 nm and 18.16 nm, respectively), and thus suggests only minor morphological changes. These observations suggest low leaching levels after 4 oxidation cycles.

3.8. Peroxidase mimetic activity of polymer supported complex

Peroxidase mimetic activity of polymer-supported complex PS-[$V^{IV}O$(sal-dahp)] (**2**) was investigated by using the typical peroxidase substrate, pyrogallol [27] in the presence of H_2O_2. The peroxidase-like

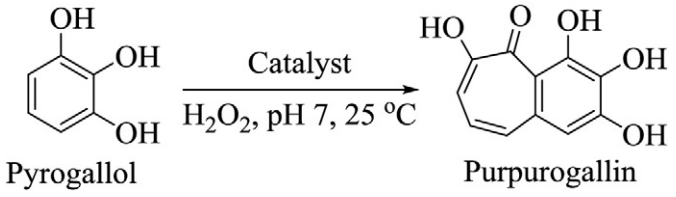

Scheme 2. Peroxidase like oxidation of pyrogallol to purpurogallin catalyzed by PS-[$V^{IV}O$(sal-dahp)] (**2**).

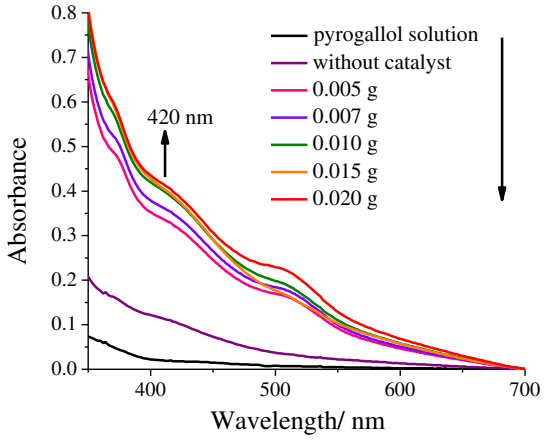

Fig. 7. Spectra of different solutions of pyrogallol obtained within 2 min after the preparation of solutions i.e. pyrogallol solution and H_2O_2 having different amounts of catalyst. Spectra of i) pyrogallol solution and ii) pyrogallol solution and H_2O_2 are also shown in figure. For experimental details see text.

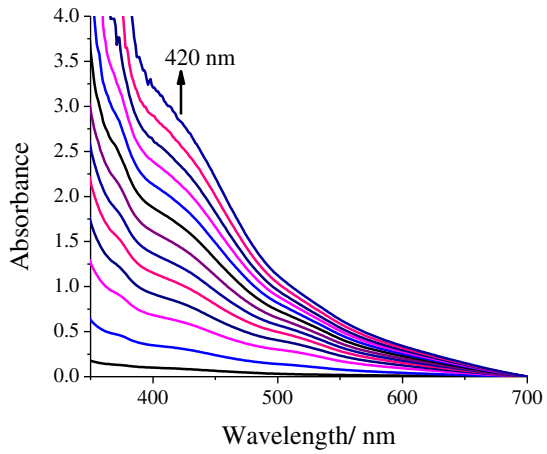

Fig. 8. Progressive increment in the absorption intensity with time, due to formation of purpurogallin. Reaction conditions: Pyrogallol solution (1 mL, 0.25×10^{-1} M) mixed with 1 mL of 30% H_2O_2 (0.25×10^{-1} M), 3 mL phosphate buffer (pH 7, 1 M) and catalyst PS-[$V^{IV}O$(sal-dahp)] (0.007 g) at 25 °C. Spectra were recorded at every 2 min time interval.

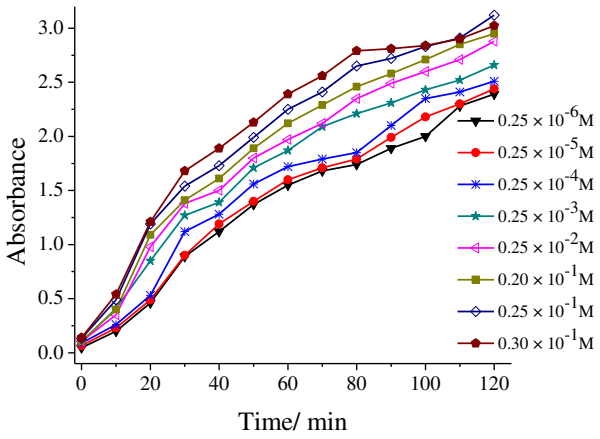

Fig. 10. Absorbance variation (at 420 nm) with time for solutions containing 1 mL pyrogallol (0.25×10^{-1} M) and different concentrations of H_2O_2 in 3 mL phosphate buffer (pH 7, 1 M) in the presence of catalyst PS-[$V^{IV}O$(sal-dahp)] (0.007 g) at 25 °C.

oxidation of pyrogallol (Scheme 2) yields purpurogallin, whose formation can be monitored by UV–visible spectroscopy.

Preliminary experiments were carried out using:

(i) 1 mL of 0.25×10^{-1} M pyrogallol in 3 mL of phosphate buffer (1 M, pH 7);
(ii) 1 mL of 0.25×10^{-1} M pyrogallol in 3 mL of phosphate buffer (1 M, pH 7) and 1 mL of 0.25×10^{-1} M solution of 30% H_2O_2;
(iii) 1 mL of 0.25×10^{-1} M pyrogallol in 3 mL phosphate buffer (1 M, pH 7), 1 mL of 0.25×10^{-1} M solution of 30% H_2O_2 and different amounts of previously swollen catalyst.

Reactions were followed by UV–visible spectrophotometry after 2 min of their preparation by measuring the formation of the oxidation product at 420 nm. The transparent pyrogallol solution turns yellow [28] in the presence of H_2O_2 showing a very weak absorption at ca. 420 nm, due to the formation of purpurogallin; Fig. 7.

Solutions of set (iii) gradually changed to pink and then to reddish-brown along with the appearance of a band at 420 nm, which was not present in the catalyst spectrum, indicating that pyrogallol can be oxidized by H_2O_2 in the absence/presence of catalyst, with the oxidation extent being different in the two cases. Furthermore, slight variations in color, along with different absorption intensities at 420 nm, could be observed for samples containing different catalyst amounts; Fig. 7. The new band at 420 nm is due to the formation of purpurogallin, which is absent in the pyrogallol spectrum [29,30]. The monitoring of the intensity of this band for the sample containing 0.007 g of catalyst showed maximum measurable absorbance within 2 h; Fig. 8. (For spectral changes between 200–700 nm, see Fig. SI–2) Further reaction optimization for maximizing pyrogallol oxidation was done by changing catalyst and oxidant amounts, and pH of the reaction.

The effect of catalyst's amount was evaluated by taking five different amounts (0.005–0.020 g) under the above reaction conditions, i.e. 1 mL of 0.25×10^{-1} M pyrogallol in 3 mL phosphate buffer (pH 7, 1 M), 1 mL of 0.25×10^{-1} M solution of 30% H_2O_2 and reaction temperature 25 °C. The plot in Fig. 9 shows that the oxidation of pyrogallol increased considerably when using 0.005 g of catalyst (compared to the uncatalyzed reaction). Increasing the catalyst's amount to 0.007 g slightly improved the activity, while only minimal gains were attained with further increase (to 0.010 g, 0.015 g or 0.020 g). However, the overall reaction time decreased; e.g. the assay with 0.020 g of catalyst showed the activity equivalent to the assay with 0.007 g catalyst within 1.5 h (data not shown). Therefore, a compromise between reaction time and catalyst amount was assumed, and other reaction conditions were optimized considering 0.007 g of catalyst.

The dependence of the pyrogallol oxidation on different amounts of oxidant was also evaluated. Thus, different H_2O_2 concentrations (from

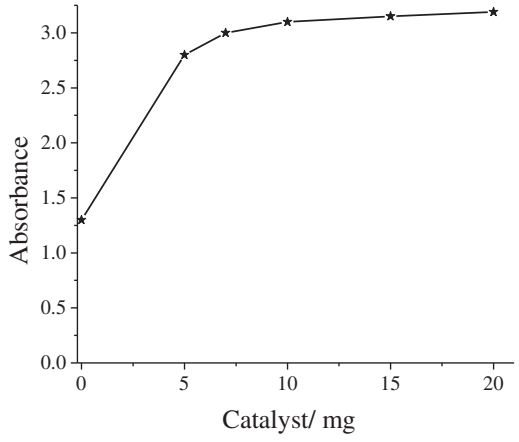

Fig. 9. Plot of maximum absorbance at 420 nm during peroxidase activity with pyrogallol measured for different amounts of catalyst. Other reaction conditions: i.e. 1 mL of 0.25×10^{-1} M pyrogallol in 3 mL phosphate buffer (pH 7, 1 M), 1 mL of 0.25×10^{-1} M solution of 30% H_2O_2 and reaction temperature 25 °C in 2 h of reaction time.

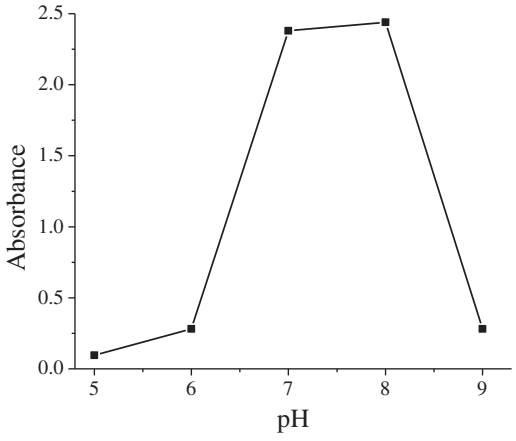

Fig. 11. Plot of maximum absorbance at $\lambda_{max} = 420$ nm at different pH values of buffer solutions (3 mL, 1 M). Other reaction conditions: pyrogallol solution (1 mL, 0.25×10^{-1} M), PS-[$V^{IV}O$(sal-dahp)] (0.007 g), 30% H_2O_2 (1 mL, 0.25×10^{-6} M) and reaction temp. (25 °C).

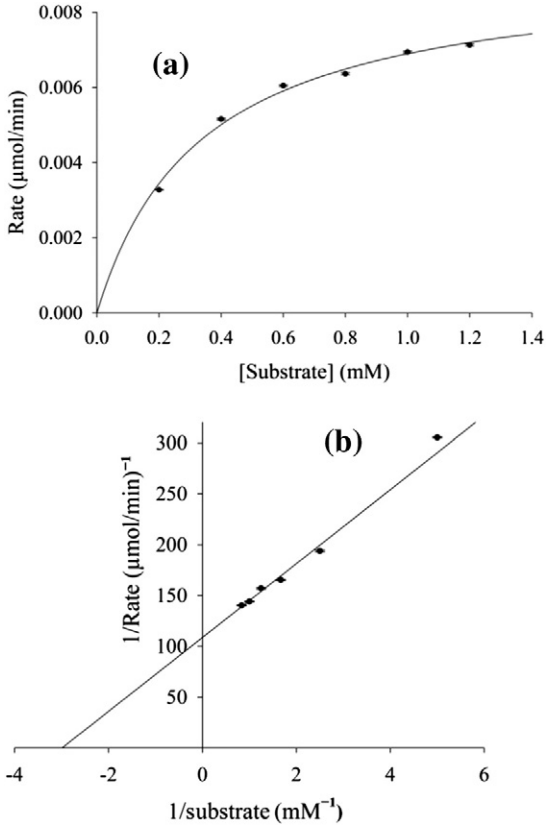

Fig. 12. Michaelis–Menten curve fit (a) for variation of pyrogallol concentration (0.2–1.2 mM) while keeping H_2O_2 (0.25×10^{-6} M) and PS-[V^{IV}O(sal-dahp)] (0.023 mg active sites mL^{-1}) concentration constant in phosphate buffer (pH7, 1 M) and corresponding Lineweaver–Burk linearization (b).

2.5×10^{-7} to 0.03 M) were considered in each set having a fixed amount of pyrogallol solution (1 mL of 0.25×10^{-1} M), catalyst (0.007 g) and pH 7 phosphate buffer (3 mL, 1 M). The reaction was monitored at 25 °C for 2 h and Fig. 10 shows the plots of absorbance at $\lambda_{max} = 420$ nm at different concentrations of H_2O_2 with time. The catalyst showed good response towards different H_2O_2 concentrations and the minimum H_2O_2 concentration used, 0.25×10^{-6} M, showed a high activity profile.

The peroxidase activity was also evaluated in buffer solutions of five different pH values. The maximum measurable absorbance at $\lambda_{max} = 420$ nm, independent of time, is shown in Fig. 11. The reaction rate was fastest at pH 8 for which maximum activity was reached within 20 min. Activity was comparatively slower at pH 7, for which maximum absorption (same value as observed for pH 8) was obtained after 2 h. For pH values 5, 6 and 9 the reaction became extremely slow and the maximum absorbance at $\lambda_{max} = 420$ nm was only ca. 0.25. Despite showing maximum activity and higher reaction rate at pH 8, pH 7 was considered optimal, since it is physiologically relevant and also environmentally similar to natural peroxidases in biological systems. Moreover, no metal leaching was observed from the polymer-supported complex at different pH values making it a versatile catalyst for different reaction environments.

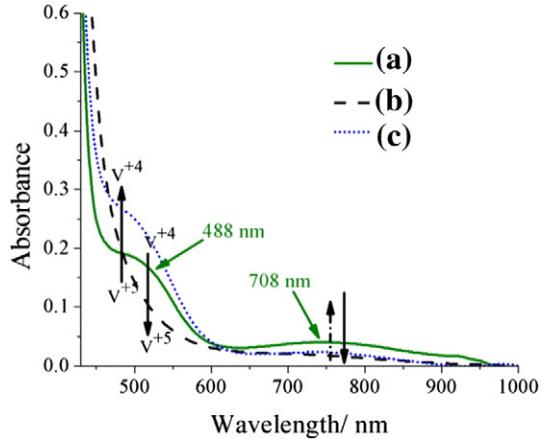

Fig. 13. Electronic absorption spectrum of (a): [V^{IV}O(Hsal-dahp)(DMSO)] (**1**) in DMF showing d-bands; (b): **1** after addition of H_2O_2 solution and (c): **1** after addition of pyrogallol solution to (b). For details of concentration of reagents refer to the text.

Additionally, catalyst **2** is recyclable up to 4 cycles (after washing with acetonitrile and drying) exhibiting roughly the same activity. In order to rule out the possibility of the peroxidase activity being due to free leached vanadyl ($[VO]^{2+}$) species, instead of the polymer-anchored complex PS-[V^{IV}O(sal-dahp)], after the catalytic runs at different pH values the reaction mixtures were analyzed by ICP–MS. No vanadium content was found demonstrating that the peroxidase mimetic activity is due to the bound PS-[V^{IV}O(sal-dahp)].

A control experiment with $VOSO_4$ (0.15 mM) (under the optimized reaction conditions) showed only a small increase in absorbance at 420 nm demonstrating the catalytic efficiency of the supported catalyst and the fact that the pyrogallol oxidation is exclusively due to the complex PS-[V^{IV}O(sal-dahp)], as there is no leaching of free vanadyl species (as shown by ICP–MS) [see Fig. SI–3]. However, it should be pointed out that at pH 7 the aqueous vanadium speciation involves the formation of hydroxide species, such as $(VO)_2(OH)_5^-$, and particularly precipitation of insoluble $VO(OH)_2$, which can account for the poor activity of $VOSO_4$.

For better understanding the peroxidase mimetic activity of PS-[V^{IV}O(sal-dahp)] kinetic parameters such as V_{max}, K_M, and K_{cat} were determined (where V_{max} is the maximum rate, K_M is the Michaelis–Menten constant and K_{cat} is the turn over frequency). For this purpose, several experiments were conducted in phosphate buffer of pH 7 (1 M) at 25 °C by varying the concentration of pyrogallol from 0.2 mM to 1.2 mM while H_2O_2 and catalyst concentrations were kept constant in all experiments (Fig. 12(A)). The reactions were carried out for 5 min and initial reaction rates were calculated by measuring the absorbance at 420 nm in kinetic mode. According to typical enzymatic kinetic assay, the reaction rates were fitted to the Michaelis–Menten Eq. (1):

$$V_i = V_{max} \times \frac{[S]}{K_M + [S]} \quad (1)$$

where V_i is the initial reaction rate, V_{max} is the maximum reaction rate, [S] is the substrate concentration and K_M is the Michaelis–Menten constant.

It was observed that for catalyst PS-[V^{IV}O(sal-dahp)] V_i follows saturation kinetics with respect to substrate concentration [S]. The rate of reaction is first-order for low substrate concentrations [S] i.e. a linear plot is obtained for V_i versus [S]. At sufficient high [S], the catalyst becomes saturated with the substrate and the rate of reaction is zero-order. Thus, PS-[V^{IV}O(sal-dahp)] follows a Michaelis–Menten behavior towards pyrogallol.

The Lineweaver–Burk plot was employed to calculate the kinetic parameters (Fig. 12(B)). The V_{max} obtained was 9.2×10^{-1} μM min^{-1} and the turn over frequency (K_{cat}) determined was 3.625×10^{-3} min^{-1}, using Eq. (2).

$$K_{cat} = \frac{V_{max}}{[\text{catalytic site}]} \quad (2)$$

Thus, we can conclude that PS-[V^{IV}O(sal-dahp)] is a suitable supported catalyst to perform the oxidation of pyrogallol in biological conditions (pH 7, aqueous medium), mimicking peroxidase activity

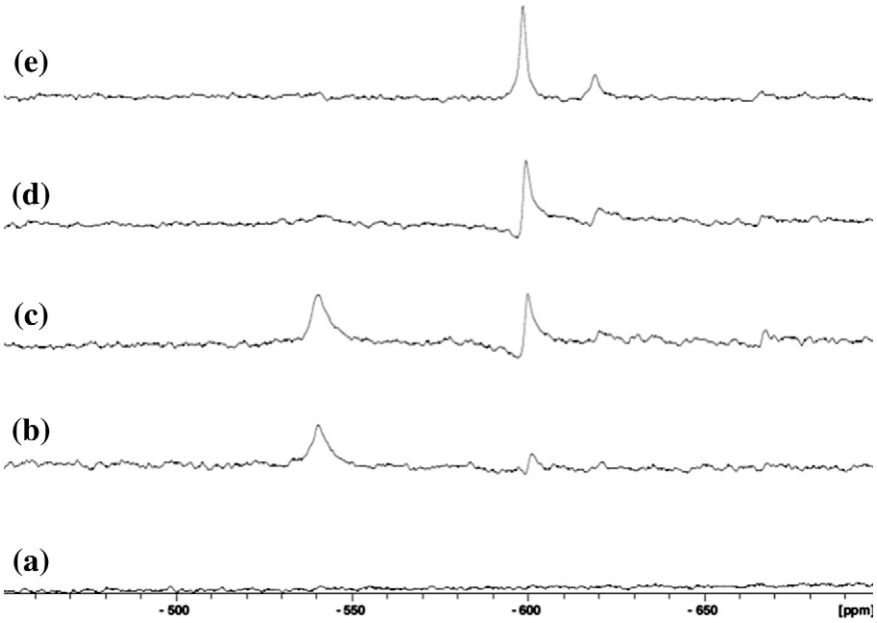

Fig. 14. ^{51}V NMR spectra measured in DMF in the following conditions: a) [VO(Hsal-dahp)(DMSO)] (1.75×10^{-3} M); b) [VO(Hsal-dahp)(DMSO)] (1.75×10^{-3} M) and H_2O_2 (4.4×10^{-3} M); c) [VO(Hsal-dahp)(DMSO)] (1.75×10^{-3} M) and H_2O_2 (1.4×10^{-2} M); d) [VO(Hsal-dahp)(DMSO)] (1.75×10^{-3} M) and H_2O_2 (1.4×10^{-2} M) and pyrogallol (1.7×10^{-3} M); e) [VO(Hsal-dahp)(DMSO)] (1.75×10^{-3} M) and H_2O_2 (1.4×10^{-2} M) and pyrogallol (3.3×10^{-3} M).

and therefore can be employed to perform environment friendly heterogeneous catalytic process.

3.9. Reactivity of [$V^{IV}O$(Hsal-dahp)(DMSO)] towards H_2O_2 and possible reaction mechanism

The stability of complex [$V^{IV}O$(Hsal-dahp)(DMSO)] was evaluated by suspending it in a mixture of acetonitrile (5 mL) and pH 8 buffer (3 mL). After 2 h under stirring the complex was recovered, dried and its IR spectrum recorded. No significant changes were observed by comparing its spectrum to that of the fresh complex, evidencing the complex's stability. Both spectra are included in Supplemental information (Fig. SI–4).

The reactivity of [$V^{IV}O$(Hsal-dahp)(DMSO)] towards H_2O_2 was studied by UV–vis absorption and ^{51}V NMR spectroscopies. The spectral changes in the absorption spectra of [$V^{IV}O$(Hsal-dahp)(DMSO)] (**1**) during the drop wise addition of a H_2O_2 solution (50 mM) show the band at 361 nm slowly disappearing. Simultaneously, two new bands appear at 310 and 398 nm, along with two isosbestic points at 340 and 395 nm (Fig. SI–5). In order to observe changes in the d–d bands, higher concentration was required and therefore DMF was used. The drop wise addition of H_2O_2 (50 mM) to [$V^{IV}O$(Hsal-dahp)(DMSO)] in DMF (5 mL of ca. 1.75×10^{-3} M solution) resulted in the slow but complete disappearance of both d–d bands at 488 and 748 nm; Fig. 13. These spectral changes indicate oxidation of V(IV) center to V(V) and plausible generation of monooxidoperoxidovanadium(V) species [$V^{V}O(O_2)$(Hsal-dahp)(DMSO)]$^{-}$. Now, addition of 3 drops of 0.25×10^{-1} M pyrogallol solution to the above mixture resulted in the appearance of both d–d bands (Fig. 13) confirming the regeneration of original oxidovanadium(IV) complex.

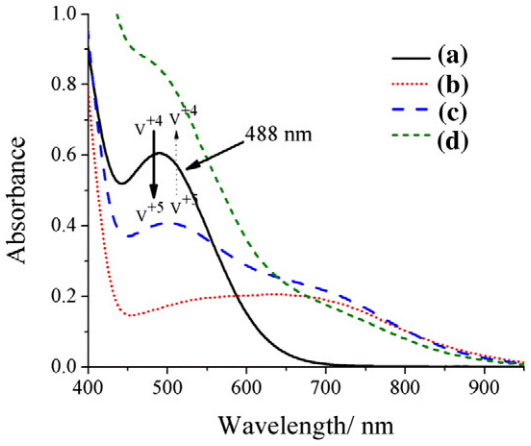

Fig. 15. Electronic absorption spectra of (a): [$V^{IV}O$(Hsal-dahp)(DMSO)] (**1**) in acetonitrile showing d-band at 488 nm; (b): **1** after addition of pyrogallol solution; (c) **1** after addition of pyrogallol and 2 drops of H_2O_2 solution, and (d): **1** after addition of pyrogallol and 6 drops of H_2O_2 solution. For details of concentration of reagents refer to the text.

These observations were corroborated by ^{51}V NMR experiments, which showed that after addition of H_2O_2 (22 μL, 50 mM) to 0.5 mL of the complex solution in DMF (1.75×10^{-3} M) two new peaks appear at −540 ppm and −600 ppm (Fig. 14). The peak at −540 ppm is in the expected range for cis-dioxovanadate complexes with N,O-ligands, [31–34] and the one at −600 ppm in the expected range for monooxidoperoxidovanadium(V) species [31,33]. The cis-dioxido species is probably a dimer of the type [($V^{V}O_2$)$_2$(Hsal-dahp)], for which resonances in the same chemical shift region have been observed [31]. Also, the ^{51}V NMR spectrum of a solution containing only the complex, which was left under air for 24 h showed the presence of the same peak (Fig. SI–6). With incremental additions of H_2O_2 both peaks increase. Addition of 20 μL of pyrogallol solution (0.25×10^{-1} M) to a solution containing the [$V^{IV}O$(Hsal-dahp)(DMSO)] complex (1.75×10^{-3} M) and excess of H_2O_2 resulted in the disappearance of the resonance at −540 ppm, an increase in the intensity of the resonance at −600 ppm and the appearance of a new peak at −622 ppm (Fig. 14). These observations suggest the regeneration of the [$V^{IV}O$(Hsal-dahp)(DMSO)] complex and the partial formation of an inorganic peroxovanadate complex, in agreement with the UV–vis absorption spectra.

During the catalytic cycle the vanadium center is in contact with either H_2O_2 followed by pyrogallol or vice-versa. Therefore, the reactivity of [$V^{IV}O$(Hsal-dahp)(DMSO)] (**1**) with H_2O_2 in the presence of pyrogallol was also studied. Changes observed by UV–vis spectroscopy are shown in Fig. 15. The concentration of complex **1** in acetonitrile

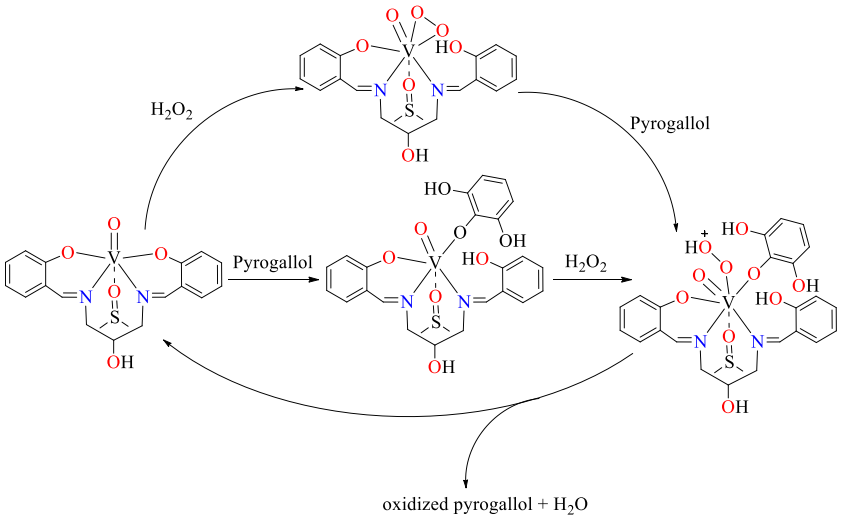

Fig. 16. Proposed catalytic cycle involved in the oxidation of pyrogallol catalyzed by [$V^{IV}O$(Hsal-dahp)(DMSO)].

was selected in order to have the 488 nm band clearly visible. Thus, drop wise addition of pyrogallol (0.25×10^{-1} M in acetonitrile) to complex **1** (0.27×10^{-3} M, 13 mL) resulted in the generation of a new band at ca. 670 nm. Simultaneously, the intensity of the 488 nm band gradually decreased and finally disappeared showing the formation of a new species, probably involving coordination of pyrogallol to the vanadium(IV) center. At this stage, the drop wise addition of a solution of H_2O_2 (50 mM H_2O_2 solution in acetonitrile) to the above mixture slowly regenerated the d–d band at 488 nm along with the flattening of the newly generated band at ca.670 nm band (Fig. 15).

Coordination of pyrogallol to the vanadium center was further corroborated by an ESI–MS study in which pyrogallol was added to [$V^{IV}O$(Hsal-dahp)(DMSO)] (**1**) in acetonitrile. The peak at m/z = 566 is assignable to the species $[V^{IV}O(\text{Hsal-dahp})(PG)K_2H]^+$. The respective ESI–MS spectrum is included in Fig. SI–7.

The lower solubility of complex **1** in acetonitrile precluded its study by ^{51}V NMR in this solvent. However, the study carried out with DMF in which the H_2O_2 solution was added to a solution containing [$V^{IV}O$(Hsal-dahp)(DMSO)] (1.75×10^{-3} M) and pyrogallol (0.3 mol equivalents), the only resonance observed was the one at −600 ppm, confirming the regeneration of $V^{IV}O$ complex, in the catalytic cycle.

All these observations suggest the detachment of pyrogallol from the vanadium center followed by its oxidation to purpurogallin after addition of H_2O_2 and regeneration of the V^{IV} species. These observations suggest that sequential addition of substrate and oxidant does not play any specific role and the transfer of oxygen to pyrogallol takes place from peroxidovanadium(V) species. Further, the metal center in the catalyst restores its oxidation state after the catalytic reaction.

^{51}V NMR spectra measured 72 h after dissolution of [$V^{IV}O$(Hsal-dahp)(DMSO)] (1.75×10^{-3} M) in DMF showed the presence of the −540 ppm peak, confirming the assignment of this resonance to the oxidation product, the dimeric cis-dioxido complex: $[(V^{V}O_2)_2(\text{Hsal-dahp})]$ (see Supplemental information, Fig. SI–6). For solutions containing H_2O_2 and pyrogallol the same resonance was present in the NMR spectra, as well as resonances at higher field (−525 and −530 ppm) corresponding probably to decomposition products. The large bandwidth of the resonances suggests the presence of organic moieties around the vanadium atom. Peroxidovanadate species usually decompose rapidly with time and its resonance appears at lower field.

Based on all these mechanistic studies, Fig. 16 has been proposed for the catalytic cycle involved in the oxidation of pyrogallol in aqueous medium by [$V^{IV}O$(Hsal-dahp)(DMSO)].

4. Conclusions

A mononuclear complex [$V^{IV}O$(Hsal-dahp)(DMSO)] has been prepared and structurally characterized. The polymer-supported complex PS-[$V^{IV}O$(sal-dahp)] was synthesized by reacting [VO^{IV}(Hsal-dahp)(DMSO)] with chloromethylated polystyrene cross-linked with 5% divinylbenzene in DMF. The supported complex was successfully applied as peroxidase mimic in aqueous medium. The oxidation of pyrogallol to purpurogallin has been achieved under mild reaction conditions at pH 7 buffered solution. Sequential addition of substrate and oxidant does not play any specific role during the catalytic reaction and oxygen transfer to pyrogallol takes place from a monoperoxidovanadium(V) species, identified in the ^{51}V NMR studies. The catalytic metal center restores its oxidation state after the catalytic reaction. Catalyst PS-[$V^{IV}O$(sal-dahp)] showed good stability over a wide pH range. Its high activity at pH 7 and recyclability without considerable decrease in activity support its application as catalyst for greener processes in industry.

Acknowledgments

Authors (MRM and NC) are thankful to the Council of Scientific and Industrial Research, New Delhi, India (Grant No. 01/(2447)/10-EMR-II) for financial support. I. Correia thanks Fundação para a Ciência e Tecnologia for Investigador FCT contract UID/QUI/00100/2013.

Appendix A. Supplementary data

Supplementary data to this article can be found online at http://dx.doi.org/10.1016/j.jinorgbio.2015.01.012.

References

[1] H.B. Dunford, Heme Peroxidases, Wiley-VCH, New York, 1999.
[2] N.C. Veitch, Phytochemistry 65 (2004) 249–259.
[3] A.T. Martinez, Enzyme Microb. Technol. 30 (2002) 425–444.
[4] A. Jaouani, F. Guillén, M.J. Penninckx, A.T. Martínez, M.J. Martínez, Enzyme Microb. Technol. 36 (2005) 478–486.
[5] R. Brigelius-Flohe, Free Radic. Biol. Med. (27) (1999) 951–965.
[6] T. Holmblad, K. Söderhäll, Aquaculture 172 (1999) 111–123.
[7] M. Zamocky, C. Jakopitsch, P.G. Furtmüller, C. Dunand, C. Obinger, Proteins: Struct. Funct. Bioinform. 72 (2008) 589–605.
[8] H.B. ten Brink, H.L. Dekker, H.E. Schoemaker, R. Wever, J. Inorg. Biochem. 80 (2000) 91–98.

[9] R. André, F. Natálio, M. Humanes, J. Leppin, K. Heinze, R. Wever, H.-C. Schröder, W.E.G. Müller, W. Tremel, Adv. Funct. Mater. 21 (2011) 501–509.
[10] M.R. Maurya, J. Costa Pessoa, J. Organometal. Chem. 696 (2011) 244–254.
[11] M.R. Maurya, A. Kumar, J. Costa Pessoa, Coord. Chem. Rev. 255 (2011) 2315–2344.
[12] A.G.J. Ligtenbarg, R. Hage, B.L. Feringa, Coord. Chem. Rev. 237 (2003) 89–101.
[13] V. Conte, A. Coletti, B. Floris, G. Licini, C. Zonta, Coord. Chem. Rev. 255 (2011) 2165–2177.
[14] J.A.L. da Silva, J.J.R. Fraústo da Silva, A.J.L. Pombeiro, Coord. Chem. Rev. 255 (2011) 2232–2248.
[15] M.R. Maurya, Curr. Org. Chem. 16 (2012) 73–88.
[16] K.I. Smith, L.L. Borer, M.M. Olmstead, Inorg. Chem. 42 (2003) 7410–7415.
[17] P. Adão, J. Costa Pessoa, R.T. Henriques, M.L. Kuznetsov, F. Avecilla, M.R. Maurya, U. Kumar, I. Correia, Inorg. Chem. 48 (2009) 3542–3561.
[18] M.R. Maurya, M. Bisht, N. Chaudhary, F. Avecilla, U. Kumar, H.-F. Hsu, Polyhedron 54 (2013) 180–188.
[19] A. Rockenbauer, L. Korecz, Appl. Magn. Reson. 10 (1996) 29–43.
[20] R.A. Row, M.M. Jones, Inorg. Synth. 5 (1957) 113–116.
[21] G.M. Sheldrick, SHELXL-97: an Integrated System for Solving and Refining Crystal Structures from Diffraction Data (Revision 4.1), University of Göttingen, Germany, 1997.
[22] K. Wüthrich, Helv. Chim. Acta 48 (1965) 1012–1017.
[23] N.D. Chasteen, in: J. Reuben (Ed.), Biological Magnetic Resonance, Plenum, New York, 1981, p. 53.
[24] A.S. Ogunlaja, W. Chidawanyika, E. Antunes, M.A. Fernandes, T. Nyokong, N. Torto, Z.R. Tshentu, Dalton Trans. 41 (2012) 13908–13918.
[25] R.S. Walmsley, A.S. Ogunlaja, M.J. Coombes, W. Chidawanyika, C. Litwinski, N. Torto, T. Nyokong, Z.R. Tshentu, J. Mater. Chem. 22 (2012) 5792–5800.
[26] Z.R. Tshentu, C. Togo, R.S. Walmsley, J. Mol. Catal. A Chem. 318 (2010) 30–35.
[27] D. Feng, Gu Z.–Y., J.-R. Li, H.-L. Jiang, Z. Wei, H.-C. Zhou, Angew. Chem. 51 (2012) 10307–10310.
[28] P.C. Pandey, A.K. Pandey, Electrochim. Acta 109 (2013) 536–545.
[29] N. Puvvada, P.K. Panigrahi, D. Mandal, A. Pathak, RSC Adv. 2 (2012) 3270–3273.
[30] H. Tauber, J. Biol. Chem. 205 (1953) 395–400.
[31] M.R. Maurya, A.A. Khan, A. Azam, S. Ranjan, N. Mondal, A. Kumar, F. Avecilla, J. Costa Pessoa, Dalton Trans. 39 (2010) 1345–1360.
[32] J. Benítez, L. Becco, I. Correia, S. Milena Leal, H. Guiset, J. Costa Pessoa, J. Lorenzo, S. Tanco, P. Escobar, V. Moreno, B. Garat, D. Gambino, J. Inorg. Biochem. 105 (2011) 303–311.
[33] D. Rehder, Bioinorganic Vanadium Chemistry, John Wiley & Sons, Chichester, 2008.
[34] M.R. Maurya, N. Chaudhary, A. Kumar, F. Avecilla, J. Costa Pessoa, Inorg. Chim. Acta 420 (2014) 24–38.